Hydrogen Tank Project Q2 Report – FY 11

KI Johnson   TA Kafentzis
KJ Alvine   ME Dahl
DC Skorski   SG Pitman
BN Nguyen

May 2011

DISCLAIMER

This report was prepared as an account of work sponsored by an agency of the United States Government. Neither the United States Government nor any agency thereof, nor Battelle Memorial Institute, nor any of their employees, makes **any warranty, express or implied, or assumes any legal liability or responsibility for the accuracy, completeness, or usefulness of any information, apparatus, product, or process disclosed, or represents that its use would not infringe privately owned rights**. Reference herein to any specific commercial product, process, or service by trade name, trademark, manufacturer, or otherwise does not necessarily constitute or imply its endorsement, recommendation, or favoring by the United States Government or any agency thereof, or Battelle Memorial Institute. The views and opinions of authors expressed herein do not necessarily state or reflect those of the United States Government or any agency thereof.

This document was printed on recycled paper.
(9/2003)

Hydrogen Tank Project Q2 Report – FY 11

KI Johnson   TA Kafentzis
KJ Alvine   ME Dahl
DC Skorski   SG Pitman
BN Nguyen

May 2011

Pacific Northwest National Laboratory
Richland, Washington 99352

Quarterly Report for PNNL – Low Cost Composite Tank Project

Topic A: Liner Materials Characterization and Testing

During this Quarter PNNL has tested 83 ASTM D638 type 3 high density polyethylene (HDPE) and Quantum liner materials samples that were subjected to high pressure hydrogen between 3,000psi and 4,200psi in order to further the understanding of the degradation effects of hydrogen exposure on the mechanical properties of polymers. For example, in the last quarter we observed a general decrease in HDPE modulus after high pressure H_2 exposure that recovered with time after removal from the hydrogen. The tests thus far have yielded 20,000 data points for our team to analyze. In an effort to more systematically analyze this data we have developed a set of excel macros to extract all pertinent information from each data set including, among many other things, the calculated hydrogen concentration (based on a simple model for hydrogen diffusion and time) in the sample at the time of testing, the sample charging conditions, and sample geometry. These pieces of data, combined with the ability to rapidly visualize any portion of the selected data within a few key strokes have allowed us to determine overall trends in the data sets.

Our original intent was to focus our analysis on the modulus values of each of the samples. However, modulus for plastics can be a challenge to measure in a repeatable manner due to the lack of a linear region at the beginning of the stress strain curve. In order to address this we have added functionality to our excel macros to allow us to calculate the chord and tangential modulus for all samples. These methods have been set-up in accordance with the ASTM E111-04 standard and are applied uniformly over all data sets during analysis. The testing methods are also designed so the user can input the targeted chord length, strain band, or stress band. Based on this input the macro will automatically determine the correct point at the beginning of the test after any slack adjustments as prescribed in annex 1 of the ASTM D638 standard. The macro will then adjust the second point accordingly in order to obtain the correct chord length. Tangential modulus can be taken at any given point or a value can be targeted to return a stress and strain coordinate. All of the results from the above calculations are integrated into the initial excel macro to allow for rapid visualization of the results. After using these tools to analyze the entire data set we realized much stronger correlations could be made between the hydrogen concentration and the ultimate tensile stress (UTS) and ultimate yield strain (UYS). We are continuing to use and refine these tools to determine if there is a repeatable effect on the modulus of the samples that have been tested.
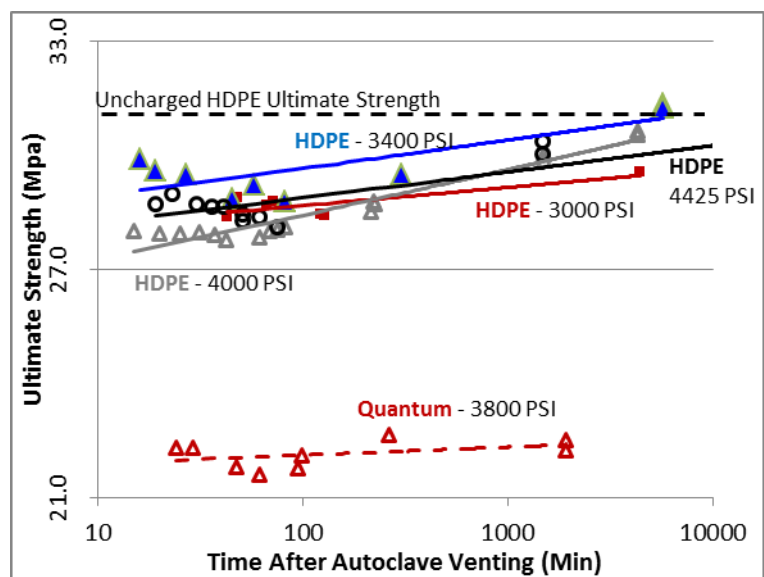

Figure 1. Ultimate Strength vs Time after Autoclave Venting for HDPE and Quantum Samples.

It appears that there may be a power law relationship between the UTS and the amount of time after autoclave venting due to hydrogen effects decreasing as hydrogen diffuses out of the samples. This trend is repeated in all of the samples of HDPE and Quantum materials and shows the samples recovering to an initial UTS value after approximately 1 day after removal from high pressure hydrogen. This is a significant finding because 15 minutes after being removed from the pressurized hydrogen environment the samples show a decrease in UTS by approximately 9% (Figure 1). Previous measurements indicated a nearly 15-20% drop in modulus over the same period.

As a quick test to measure the impact of crystallinity on the hydrogen degradation we also ran hydrogen charging tests on some low density polyethylene (LDPE) which is nearly identical to HDPE except that it has a much lower crystalline content. A similar decrease of 10% of UTS was observed in the LDPE material. The LDPE was unique in that the samples never recovered to their full strength and macro blisters began to appear inside the material as the samples sat in ambient conditions. While the HDPE material from both McMaster and Goodfellow show a similar decrease of approximately 9%, the Quantum material only shows a decrease of approximately 2%. Furthermore the Quantum material appears to recover to its initial value faster than the other materials tested. Thus we can conclude that higher crystalline content and cross-linking is essential for hydrogen compatibility as evidenced by the poor performance of the LDPE and the improved performance of the Quantum material (which is highly cross-linked) over the HDPE.

Not surprizingly there also appears to be a similar power law like dependence on the ultimate yeild strain (UYS) of the samples after being removed from the pressurized hydrogen environment. This indicates a higher elongation at a lower load for the samples. This relationship was also found to be repeatable across the HDPE, Quantum, and Goodfellow samples. The results from the HDPE tests are shown in Figure 2. The LDPE samples again did not agree with the overall trend and showed a continuing increase in UTS with increasing time after exposure. It is unclear if these

Figure 2. Ultimate Yield Strain vs Time After Autoclave Venting for Quantum and HDPE Samples

samples stabilize at an increased value over time and testing is ongoing. Again the Quantum samples showed a smaller change than the commercial HDPE samples, ~9% increase vs. ~30% increase respectively.
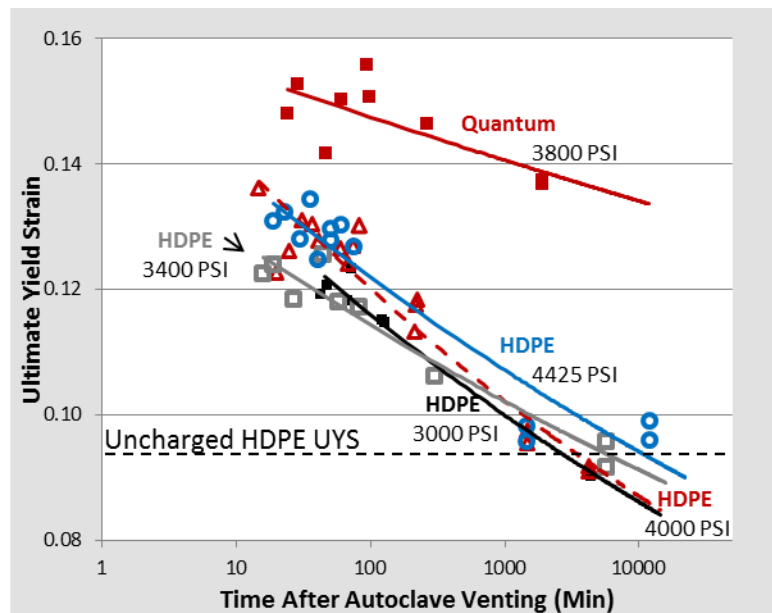
As a final note on the LDPE testing, we remark that LDPE samples are irreversibly affected when subjected to high pressure hydrogen environments which is different behavior from the materials tested. After prolong exposure in ambient conditions the LDPE begins to show macro blistering inside the plastic. Examples of these blisters are shown in Figure 3.
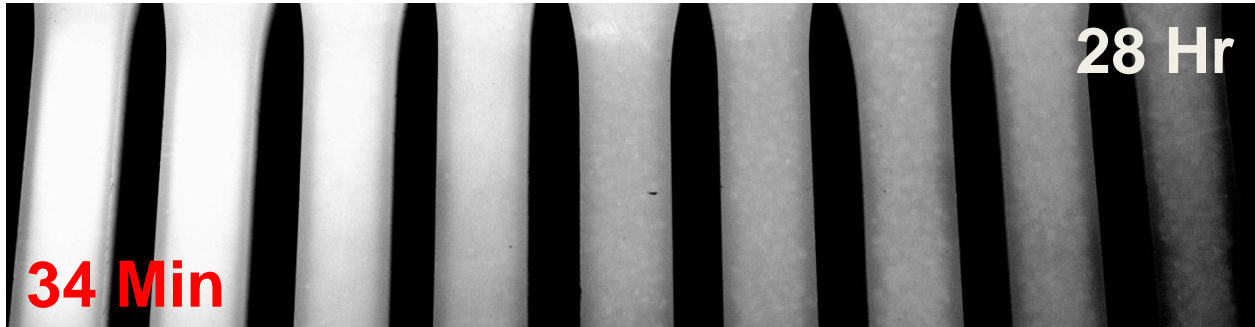

28 Hr

34 Min

Figure 3. Graphic showing the progression of blistering formation in McMaster LDPE with time after removal from high pressure H2.

Topic B: Design and build of an in-situ tensile rig for high pressure H$_2$.

One noted limitation in our previous tensile testing of liner materials is the inherent ex-situ nature of the testing itself. We have been able to charge materials under high pressure H$_2$ and test them in a standard tensile set-up as a function of time while the H$_2$ diffuses out. Our minimum test time is severely limited by the time it takes to vent the autoclave from several thousand psi down to ambient, followed by inert gas purges, removal of the autoclave bolts, transport of the samples to the tensile rig, and sample loading on the instron load frame. We have been able to optimize the process down to a minimum time of 15-20 minutes but it is unlikely we will be able to reduce this further. While this does yield valuable information about what the liner material experiences after the tank is depressurized, it cannot give us true in-situ results where

Figure 5: (RIGHT) The high pressure hydrogen autoclave can accommodate up to 5" diameter x 10" height. (LEFT) A photograph of the partially completed in-situ tensile rig. LVDT is not shown.

the tank is under pressure. In order to address this point we have designed and built a simple in-situ tensile rig to be operated within our autoclaves and pull liner samples under high pressure H$_2$ (Figure 5).

Hydrogen materials compatibility and space limitations played an important role in the design criteria for this in-situ tensile rig. In order to pull relatively small ¼" thick samples we require a load frame capable of pulling at least 100 lbs of force. In addition we need to be able to measure the load and the sample displacement, all within space limitations of 5" diameter by 10" in height. While there are commercially available mini-tensile rigs available, these are relatively expensive and rely on rare-earth magnet based motors to generate load. Previous testing with rare-earth motors reveals that these motors fail rapidly when exposed to high pressure hydrogen. This is most likely due to the formation of Nd hydrides that swell the internal motor components, jamming the motor. Replacement of the rare-earth based motors was considered. However, the alternative was brushed AlNiCo motors. While we expect that these motors would not have the issues of hydride formation, it was decided that deliberately introducing a spark source into the high pressure hydrogen environment was inadvisable. Brushless AlNiCo or ferrite based motors were found at a third party, but were relatively expensive and large for our application. Based on these considerations we have instead decided to use a solenoid based system to generate the required load. Solenoids remove both the sparking and the hydride forming issues and are relatively in-expensive.

The solenoid provides up to 120lbs of force to pull a polymer specimen. The extension of the sample is measured with an LVDT and the load is measured with a special capacitive load cell designed with a reference cell to overcome any issues with the hydrogen atmosphere. As part of the build the solenoid was tested on a standard load frame and was found to be able to pull small HDPE samples within an appropriate time frame based on a constant current supply. Eventually the load will be more precisely controlled with a programmable current source due to the nearly exponential increase in the load as the solenoid core is retracted. The in-situ mini tensile rig is currently in the final stages of assembly and electrical hook-up to the wiring harness on the autoclave. A shake-down period of testing and calibrating the individual components under high pressure H_2 and in air will be completed in the next quarter, followed by in-situ testing of polymer samples under high pressure H_2. Samples will include both standard HDPE and Quantum liner materials.

Topic C. Stress Analysis of Tank Layup Patterns and Alternate Matrix Materials

During this quarter, we applied a recently developed multiscale materials model to analyze the filament-wound composite hydrogen storage tanks. The purpose of this work was to predict the tank burst pressure as a function of the tank layup and the mechanical properties of the epoxy matrix. The ABAQUS finite element code was enhanced to include the EMTA-NLA multi-scale nonlinear materials model. EMTA-NLA is based on the incremental Eshelby-Mori-Tanaka approach and it acts as a user subroutine in ABAQUS. It was developed by PNNL under the DOE Vehicle Lightweight Materials Program for discontinuous fiber polymer materials [1] and has recently been expanded to continuous fiber composites to analyze filament-wound composite pressure vessels [2].

EMTA-NLA spans three modeling scales. The microscale considers the unidirectional continuous elastic fibers embedded in an elastic-plastic matrix that obeys the Ramberg-Osgood relation and J_2 deformation theory of plasticity. The mesoscale behavior representing the composite lamina is obtained through an incremental Mori-Tanaka model and the Eshelby inclusion method. The implementation of

the micro-meso constitutive model in ABAQUS allows a filament-wound composite pressure vessel (macroscale) to be analyzed including the nonlinear stress-strain response of the composite as it approaches the burst condition. Failure of the composite lamina is predicted by a criterion that accounts for the strengths of the fibers and the matrix as well as of their interfaces. The predicted burst pressures for the different tank layups agree well with Quantum's experimental results. Furthermore, the analysis shows that using a stronger and stiffer epoxy matrix material would significantly improve the tank burst pressure.

Figure 6 shows the epoxy matrix uniaxial stress-strain curves used in the analyses. These are described by the Ramberg-Osgood relation in terms of the total matrix equivalent stress ($\overline{\sigma}_m$) and strain ($\overline{\varepsilon}_m$):

$$\overline{\varepsilon}_m = \frac{\overline{\sigma}_m}{E_m} + (\frac{\sigma_0}{E_m})(\frac{\overline{\sigma}_m}{\sigma_0})^n \tag{1}$$

where E_m is the matrix elastic modulus, σ_0 and n are the reference stress and the power-law exponent. Based on Quantum's lamina elastic properties and a literature review on epoxy resins, the curves for epoxies numbered 1 and 2 represent high mechanical performance epoxies suitable for compressed hydrogen tank applications. Epoxy 2 is 57 % stiffer and has 33% higher tensile strength than Epoxy 1.
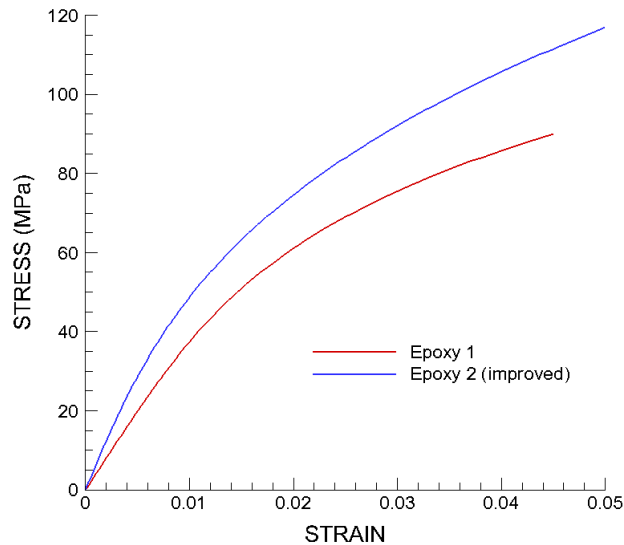

Figure 6. Epoxy uniaxial elastic-plastic stress-strain responses used in the analysis.

ABAQUS/EMTA-NLA analyses were performed for the Quantum/Boeing tanks numbered 1, 5, and 7 using Epoxy 1. Reverse engineering with EMTA-NLA showed that Epoxy 1 has mechanical properties close to those for the actual epoxy used in these tanks. The cylindrical bodies of the tanks were modeled using the composite layered shell elements in ABAQUS. The shell layers were modeled using the elastic-plastic and strength model in EMTA-NLA. The action of the dome was replaced by an axial load

distribution at one end of the tank equal to $P\pi R_{in}^2$ where P is the internal pressure and R_{in} is the internal tank radius.

Figure 7 shows the predicted evolution of the failure criterion in different layers versus tank pressure obtained in the Tank 1 analysis. The failure criterion in all layers first evolves slowly with the pressure, but it increases quickly when the pressure has exceeded about 40 MPa. At a given pressure, the failure criterion values are higher in the helical layers than in the hoop layers, particularly in the helical layers oriented away from the hoop direction. Failure of the tank is predicted to be caused by failure of the helical layers that lead the hoop layers to failure. All the layers have failed when the tank pressure reached 149.6 MPa.
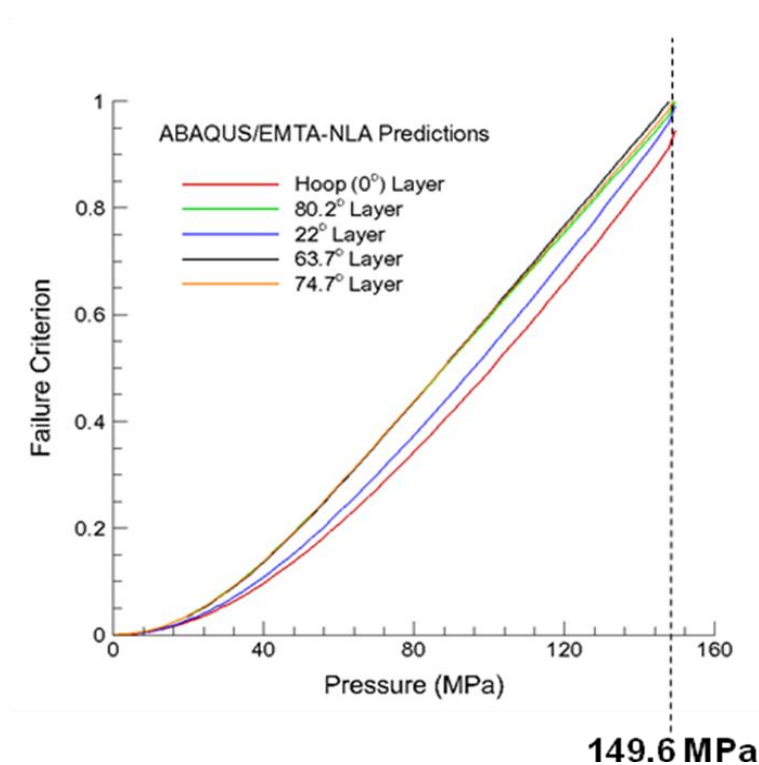

Figure 7. Predicted failure criterion vs tank pressure in selected helical & hoop layers of Tank 1.

Figures 8 and 9 report the results for Tanks 5 and 7. These tanks do not have the helical layers oriented between 0 degree and 70 degrees with respect to the hoop direction (0 degree layers). Tank 5 is the thinnest (9.76 % thinner than Tank 1) while Tank 7 is about 7.3% thinner than Tank 1. Figures 8 and 9 show that the evolutions of the failure criterion in the helical layers (oriented between 70 and 80 degrees) are practically identical, and the failure criterion is higher in the helical layers than in the hoop layers. That explains why the helical layers fail first, and their failure leads to failure of the hoop layers. The absence of the helical layers oriented less than 70 degrees has a beneficial effect: Tank 7 is 7.3 % thinner than Tank 1 but has a predicted burst pressure quite close to the value for Tank 1. Table 1 summarizes the predicted and experimental values of the burst pressures for these tanks. Tank 5 has the lowest burst pressure. The ABAQUS/EMTA-NLA predictions agree well with the experimental burst

pressure trend as a function of the layup. It is noted that the agreement is only qualitative as the actual constituent properties for the analyses were not known and were approximated for all the analyses.

The model was also used to shows the benefit of using a stronger and stiffer epoxy on increased burst pressure. The ABAQUS/EMTA-NLA analysis was conducted for the Tank 1 layup using Epoxy 2 whose stress-strain response is illustrated on Figure 1. All other parameters including the layup were unchanged. Figure 5 reports the tank pressure as a function the hoop strain for Tank 1 with Epoxy 1 and Epoxy 2. A burst pressure of 166.6 MPa was predicted for Epoxy 2 compared to 149.6 MPa for Epoxy 1.
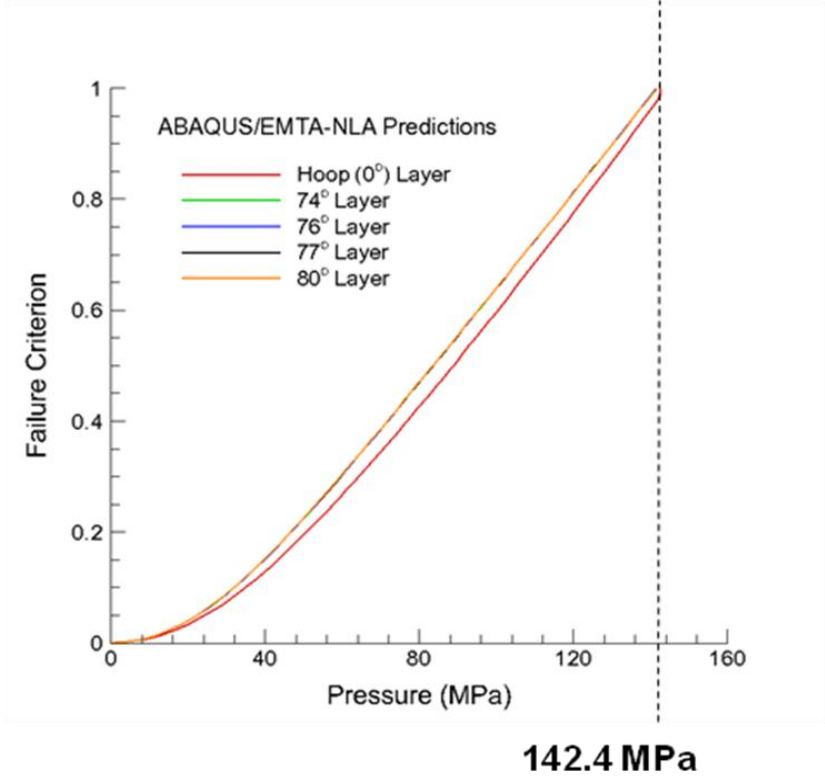

Figure 8. Predicted failure criterion vs. tank pressure in selected helical & hoop layers of Tank 5.
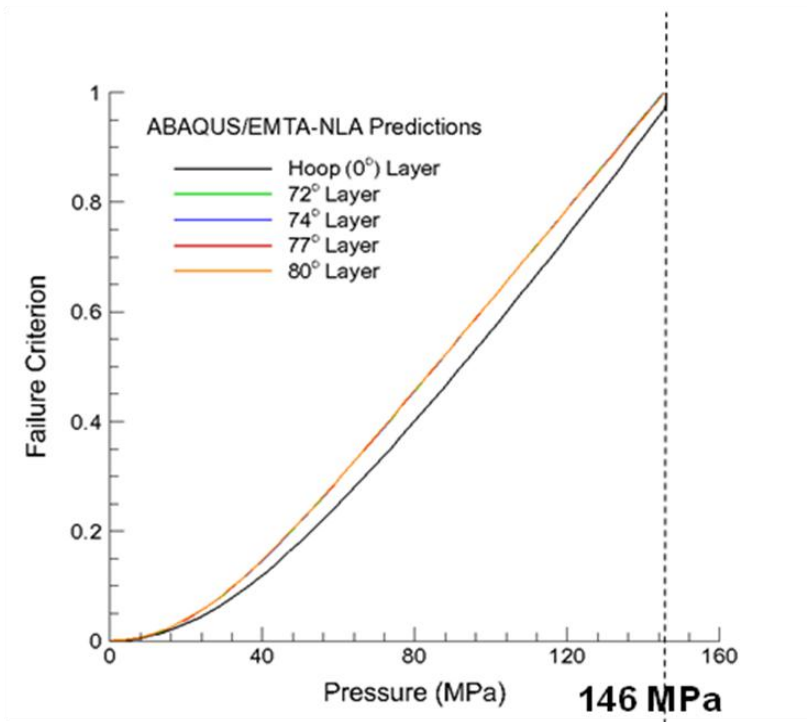
Figure 9. Predicted failure criterion vs. tank pressure in selected helical & hoop layers of Tank 7.

	Burst Test MPa (ksi)		Predictions MPa (ksi)		
Tank 1	163.9 (23.77)	100%	149.6 (21.70)	100%	
Tank 5	141.3 (20.50)	86.24%	142.4 (20.65)	95.19%	
Tank 7	158.1 (22.93)	96.47%	146 (21.18)	97.59%	

Table 1. **Experimental and predicted burst pressures for Tanks 1, 5, and 7.**
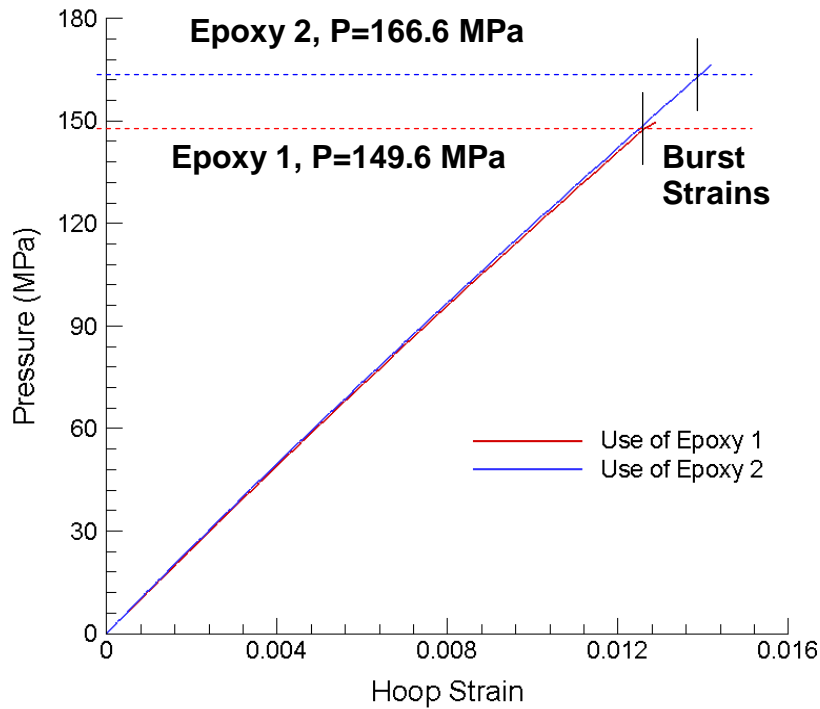
Figure 10. Predicted pressure vs. hoop strain for the Tank 1 layup with Epoxy 1 and Epoxy 2.

Topic D. Cost Analysis of Tanks 1 and 7

The cost analysis was updated to compare Tanks 1 and 7 which both exceeded the required burst pressure of 22.85 ksi. Tank 1 saved 11.1 kg of the 76 kg baseline filament wound tank for a 14.6% weight savings. Further optimization of the Tank 7 design saved an additional 6.3 kg for a 22.9% weight savings compared to the baseline tank. Both of these tanks were produced with single layers of advanced fiber placed composite in the dome sections. Tank 1 applied the composite tape directly to the HDPE liner ends. Tank 7 was fabricated by applying the composite tape on foam molds of the tank ends, transferring these dome reinforcements to the tank liner and over-wrapping with filament wound material. Exceeding the required burst pressure showed that the dome reinforcement could be made in a parallel manufacturing cell rather than requiring that advanced fiber placement be combined directly in the filament winding cell. Table 2 shows that, compared to fully integrated manufacturing, fully separate (parallel) manufacturing reduces the manufacture time from 8.2 hours to 4.3 hours. This reduces the required number of filament winding cells by 48% and the number of advanced fiber placement cells by 52% (for 500,000 units per year). This represents a $30 per tank in manufacturing cost. Table 2 also shows that the improved performance of Tank 7 has increase the specific energy from 1.5 to 1.78 kWhr/kgH$_2$ and the reduced the tank cost from $23.45 to $20.80 per kW-hr.

Summary Table		Baseline 129L	Tank 1 Layup		Tank 7 Layup	
		Type IV Tank	Hybrid FW + AFP Reinforced		Hybrid FW + AFP Reinforced	
			Fully Integrated	Separate	Fully Integrated	Separate
		Filament Wound	FW and AFP	FW and AFP	FW and AFP	FW and AFP
Composite Mass, kg	FW	76	63.4	63.4	56.23	56.23
	AFP		1.5	1.5	2.4	2.4
Total Composite Mass, kg		76	64.9	64.9	58.63	58.63
Total Place Time, hr/tank		5.75	7.27	4.80	8.21	4.25
# Manuf. Cells for 500K/yr	FW	191	242	159	273	142
	AFP		484	165	546	264
Tank Costs						
FW Composite		$2,290	$1,910	$1,910	$1,694	$1,694
AFP Composite			$90	$90	$145	$145
End Boss		$250	$250	$250	$250	$250
Manuf. Equipment		$36	$66	$41	$72	$45
Factory Space		$7	$10	$7	$11	$8
Total Tank Cost		$2,583	$2,326	$2,299	$2,171	$2,141
% Tank Cost Savings		0%	10%	11%	16%	17%
DOE Measures						
Specific Energy, kWh/kg 1		1.50	1.67	1.67	1.78	1.78
Cost Efficiency, $/kWh 2		$23.45	$21.91	$21.75	$20.98	$20.80
1 5 kg H2 * 33.31 kWh/kgH2 / (Tank+OtherComponents+H2 mass, kg) OtherCompMass=30kg						
2 (Tank+OtherComponents $$) / (5 kg H2 * 33.31 kWh/kgH2)						

Table 2. Comparison of Tanks 1 and 7 to the baseline filament wound tank.

References

[1] Nguyen BN, Bapanapalli SK, Kunc V, Phelps JH, Tucker III CL. Prediction of the elastic-plastic stress/strain response for injection-molded long-fiber thermoplastics. Journal of Composite Materials 2009; 43: 217-246.

[2] Nguyen BN and Simmons KL (2011). "A Multiscale Modeling Approach to Analyze Filament-Wound Composite Pressure Vessels (submitted).